

# Towards a physical comprehension of material strengthening factors during macro to micro-scale milling

M. Asad, T. Mabrouki, F. Girardin, Y. Zhang, J.-F. Rigal

Université de Lyon, CNRS, INSA-Lyon, LaMCoS, UMR5259., F69621, France,

E-mail: asad.muhammad, tarek.mabrouki, francois.girardin, yancheng.zhang, Jean-Francois.Rigal@insa-lyon.fr

**crossref** <http://dx.doi.org/10.5755/j01.mech.17.1.210>

## 1. Introduction

Worthy scientific researches have been made in past for the physical comprehension of the size effect phenomenon in the domain of micro cutting processes [1-3]. The term size effect in machining is usually attributed to define the nonlinear increase in specific cutting energy (SCE) when uncut chip thickness ( $h$ ) decreases to few microns. Numerous investigations have shown that there are multiple factors that can increase material strength and contribute to the size effect in micro machining operations. From material point of view, Backer et al. [1] attributed the size effect to the reduction in material imperfections when deformation takes place on small volume. While, Larsen-Basse and Oxley [2] highlighted the importance of the increase in strain rate in primary shear zone with a decrease in uncut chip thickness, as the primary cause in increasing material strength. Dinesh et al. [3] explained the increase in hardness of metallic materials with the decrease in deformation depth, as the consequence of the strong dependence of flow stress on strain gradient (SG) in the deformation zone. Based on their work Joshi and Melkote [4] had presented an analytical model for orthogonal cutting incorporating SG effects in material constitutive law.

It have also been reported in previous researches that the cutting tool edge radius is the major cause of size effect [5, 6]. In this regard Nakayama and Tamura [6] believe that, as  $h$  reduces to micrometric level, tool edge radius becomes comparable or some times greater than chip thickness. Under these conditions shear plane angle becomes very small leading to greater plastic energy dissipations in the workpiece subsurface. Liu and Melkote [7] have recently shown in their numerical work that plastic shear zone generated by an edged radius tool is more expanded and widened when compared with the one produced by a sharp tool. This in turn requires higher energy dissipation, hence contributing to the size effect. Other researchers [8, 9] believe in the existence of ploughing forces associated with the frictional rubbing and ploughing mechanism as the main reason of increase in SCE with decrease in uncut chip thickness. Some researches had attributed the size effect to an increase in shear strength of the workpiece material due to a decrease in tool-chip interface temperature as  $h$  decreases [10, 11]. In this context, Liu and Melkote [10] showed in their recent micro cutting simulation work that the decrease in secondary deformation zone temperature contributes dominantly to the size effect as  $h$  decreases.

Nevertheless, in literature most of the studies concerning tool-workpiece interaction [12, 13] are based on mechanistic modelling approach, which can not explain satisfactorily the physics of size effect phenomenon, as  $h$

decreases from macro to micro level. Only a few studies have been made using FE method [10, 11]. In this framework the present contribution put forwards a numerical approach based on FE method to study the dominance of strain hardening characteristics, in increasing material strength. The case of down-cut milling process where the  $h$  decreases from macro to micro level dimensions was treated. The phenomenological reason explaining on the one hand that how material strain hardening characteristics influence the size effect and on the other hand the nonlinear increase in SCE for a particular  $h$  value has been addressed. Moreover, to study the contribution of SG on the size effect under high cutting speeds, modified Johnson-Cook (JC) expression of the equivalent stress [14] (incorporating SG-based plasticity approach) has been formulated in ABAQUS<sup>®</sup>/EXPLICIT via its user subroutine VUMAT. Milling experiments have been carried out to compare the numerical results of SCE and chip morphology.

## 2. Finite element modelling

### 2.1. Geometrical model and hypothesis

A FE based numerical model for 2D orthogonal down cut peripheral milling case for an aluminium alloy A2024-T351 has been conceived in ABAQUS<sup>®</sup>/EXPLICIT software (version 6.7.1). To simplify the problem of cutting to 2D case many assumptions have been made and which can be summarised as follows.

- Helix angle for the used insert is small,  $\lambda_s = 9^\circ$ . This angle does not affect too much on  $F_z$  (force component along tool axis of rotation). For the studied cutting speeds,  $F_z$  was noted less than 10% of the total applied force  $\overline{F_{tot}}$ , and can be ignored. Therefore, axial depth of cut (workpiece thickness,  $a_p = 4$  mm) may be assumed to be constant.
- As diameter of milling tool ( $D_T = 22$  mm) is greater than workpiece deformation area (chip and cutter path zone), therefore, the deformed area can be considered as a case of orthogonal machining process as shown in Fig. 1, which demonstrates a schematic representation of the 2D down-cut peripheral milling model with mesh densities (optimal mesh 15 - 40  $\mu\text{m}$ ) at various  $h$  values and tool-workpiece boundary conditions. The pre-cited assumptions have also been adopted by Xinmin et al. [14] in building their numerical model for orthogonal micro milling process simulation.

The conceived FE model is based on quadrilateral continuum elements CPE4RT with which it was possible to perform a coupled temperature-displacement calcula-

tions [15]. A relatively lower value of feed rate  $f$  when compared with the axial cutting depth  $a_p$ , had allowed to perform plane strain calculations. The geometrical model concerning the present study is presented in (Fig. 1).

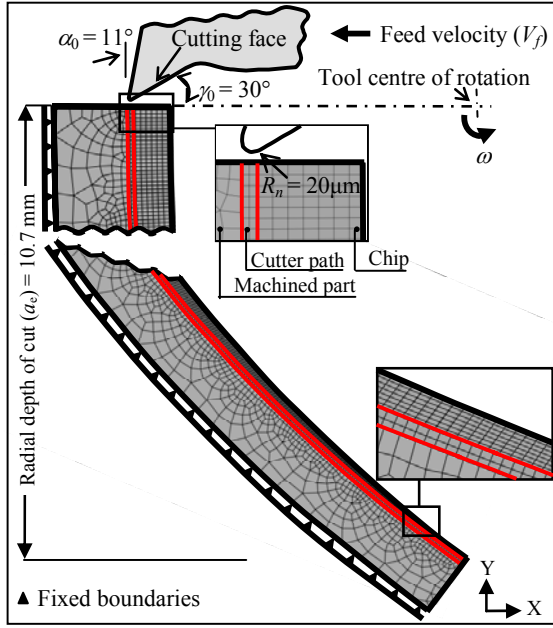


Fig. 1 Tool-workpiece geometrical model and boundary conditions

The thickness of cutter path band was assumed to the order of tool edge radius ( $R_n = 20 \mu\text{m}$ ) [16]. For the present study, a macro milling tool with the diameter of  $D_T = 22 \text{ mm}$  was used. Its geometry is exactly the same as that had been used in experimentation (shown later in section 3) with a rake angle  $\gamma_0 = 30^\circ$  and a flank angle  $\alpha_0 = 11^\circ$ . The tool has been modelled as rigid body and all the boundary conditions were applied to its centre of rotation so that it can advance with feed velocity  $V_f$  (feed rate  $f = 0.2 \text{ mm/tooth}$ ) in negative  $x$ -axis direction. It can also rotate in anti-clockwise direction with an angular velocity  $\omega$ , whereas the rest degrees of freedom have been blocked for tool motion. As the tool rotates and advances simultaneously, the cutter traces a trochoidal path. This produces a chip of variable section in milling process. Trochoidal path set given by Eq. (1) was used to model milling-cutter path (chip separation zone) and chip section geometry.

$$\left. \begin{aligned} P_{x(i)}(t) &= V_f t + \frac{D_T}{2} \cos\left(\frac{2i\pi}{z_t} + \omega_r t\right) \\ P_{y(i)}(t) &= \frac{D_T}{2} \sin\left(\frac{2i\pi}{z_t} + \omega_r t\right) \end{aligned} \right\} \quad (1)$$

where  $P_{x(i)}$  and  $P_{y(i)}$  are  $x$  and  $y$  coordinates of the  $i$ th tooth of the milling tool ( $i = 1, 2, \dots, z_t$ , where  $z_t$  is the total number of tool teeth) and  $t$  is the cutting time.

In the present study, Zorev's stick-slip friction model [17] being one of the most commonly used approximations for frictional contact between the chip and tool for a critical shear stress of 203 MPa has been used. Whereas an average friction coefficient 0.17; as measured by Ni et al. [18] on pin-on-disk tests using a high temperature tribometer for diamond-like carbon coatings against

aluminum alloys, has been assumed in all simulations.

## 2.2. Material behaviour law

The constitutive material model equations are the same as those used in previous research works [14, 19]. However, some details have to be mentioned in the present contribution. Indeed, the material behaviour model without considering SG is the one proposed by JC [20] presented by the expression of the equivalent stress (Eq. (2)).

$$\bar{\sigma}_{JC} = \left( A + B \bar{\epsilon}^n \right) \left[ 1 + C \ln \left( \frac{\dot{\bar{\epsilon}}}{\dot{\bar{\epsilon}}_0} \right) \right] \left[ 1 - \left( \frac{T - T_r}{T_m - T_r} \right)^m \right] \quad (2)$$

where  $A$  is the initial yield stress,  $B$  is the hardening modulus,  $C$  is the strain rate dependency coefficient,  $m$  is the thermal softening coefficient,  $n$  is the work-hardening exponent,  $T$  is the temperature at a given calculation instant,  $\bar{\epsilon}$  is the equivalent plastic strain,  $\dot{\bar{\epsilon}}$  is the plastic strain rate and  $\dot{\bar{\epsilon}}_0$  is the reference strain rate.

In the proposed numerical model, chip formation is realised in two steps. The first step concerns the damage initiation, whereas the second one concerns damage evolution.

*Damage initiation step:* The JC shear failure model (Eq. (3)) is used as a damage initiation criterion.

$$\bar{\epsilon}_{0i} = \left[ D_1 + D_2 \exp \left( D_3 \frac{p}{\bar{\sigma}} \right) \right] \left[ 1 + D_4 \ln \left( \frac{\dot{\bar{\epsilon}}}{\dot{\bar{\epsilon}}_0} \right) \right] \times \left[ 1 + D_5 \left( \frac{T - T_r}{T_m - T_r} \right) \right] \quad (3)$$

where  $D_1, \dots, D_5$  are the coefficients of JC material shear failure initiation criterion,  $p$  is the hydrostatic pressure,  $\bar{\sigma}$  is the von Mises equivalent stress and  $p/\bar{\sigma}$  is the stress triaxiality.

Damage is initiated when the scalar damage parameter  $\omega_{0i}$  exceeds 1, based on equation (4).

$$\omega_{0i} = \sum \frac{\Delta \bar{\epsilon}}{\bar{\epsilon}_{0i}} \quad (4)$$

where  $\Delta \bar{\epsilon}$  is the equivalent plastic strain increment and  $\bar{\epsilon}_{0i}$  plastic strain at damage initiation.

*Damage evolution step:* Hillerborg et al. [21] fracture energy proposal is used in ABAQUS<sup>®</sup>/EXPLICIT to reduce mesh dependency by creating a stress-displacement response after damage initiation. The fracture energy  $G_f$  required to open unit area of crack is defined as a material parameter. With this approach, the material softening response after damage initiation is characterized by a stress-displacement response which requires the definition of a characteristic length  $L$  assumed to the square root of the integration point element. According to this law, the damage evolution law can be specified in terms of fracture energy dissipation  $G_f$ . The law could be defined in the form a scalar stiffness degradation parameter  $D$  that can evolve linearly (Eq. (5)) used for cutter path section or exponentially (Eq. (6)) used for chip section.

$$D = \frac{L\bar{\epsilon}}{\bar{u}_f} = \frac{\bar{u}}{\bar{u}_f} \quad (5)$$

$$D = 1 - \exp\left(-\int_0^{\bar{u}} \frac{\bar{\sigma}}{G_f} d\bar{u}\right) \quad (6)$$

Where  $\bar{u}$  is the equivalent plastic displacement and  $\bar{u}_f$  is the equivalent plastic displacement at failure given by:

$$\bar{u}_f = \frac{2G_f}{\sigma_y} \quad (7)$$

In ABAQUS<sup>®</sup>, an element is removed from the mesh if all of the section points at any one integration location have lost their load-carrying capacity ( $D = 1$ ). Thus chip detachment is realised from the workpiece. JC laws material entities used in the numerical model are specified in Table 1 [22]. Thermo-mechanical properties of the material are given in Table 2 [23, 24].

Table 1

Johnson-Cook material behaviour and damage parameters for A2024-T351 [22]

| A, MPa | B, MPa | n    | C      | m | D <sub>1</sub> | D <sub>2</sub> | D <sub>3</sub> | D <sub>4</sub> | D <sub>5</sub> |
|--------|--------|------|--------|---|----------------|----------------|----------------|----------------|----------------|
| 352    | 440    | 0.42 | 0.0083 | 1 | 0.13           | 0.13           | -1.5           | 0.011          | 0              |

Table 2

Workpiece thermo-mechanical properties [23]

| Physical parameters   | Workpiece (A2024-T351)  |
|---|---|
| Density $\rho$ , kg/m <sup>3</sup>                                    | 2700  |
| Young's modulus $E$ , MPa   | 73000   |
| Shear modulus $G$ , MPa   | 28000   |
| Taylor's constant $\alpha$  | 0.5 [24]  |
| Burgers vector $b$ , nm   | 0.283 [24]  |
| Geometric factor (GNDs) $\chi$  | 0.3 [4]   |
| Nye factor $\bar{r}$  | 2 [14]  |
| Taylor factor $M_t$   | 3.06 [26]   |
| Poisson's Ratio $\nu$   | 0.33  |
| Fracture energy $G_f$ , N/m   | 20000   |
| Specific heat $C_p$ , Jkg <sup>-1</sup> °C <sup>-1</sup>              | 0.557 $T$ + 877.6   |
| Expansion coefficient $\alpha_d$ , $\mu\text{m.m}^{-1}\text{°C}^{-1}$ | 8.910 <sup>-3</sup> $T$ + 22.2  |
| Thermal conductivity $\lambda$ , W m <sup>-1</sup> C <sup>-1</sup>    | 25 ≤ $T$ ≤ 300:<br>$\lambda = 0.247 T + 114.4$<br>300 ≤ $T$ ≤ $T_m$ :<br>$\lambda = -0.125 T + 226$ |
| Melting temperature $T_m$ , °C  | 520   |
| Room temperature, $T_r$ , °C  | 25  |

In order to consider the SG-strengthening effects on the size effect phenomenon in machining, Xinmin et al. [14] proposed a new expression of the equivalent stress based on SG- plasticity theory. The framework of their proposed constitutive equation is expressed as

$$\sigma = f(\sigma_{ref}, \eta) \quad (8)$$

where  $\bar{\sigma}_{ref} = \bar{\sigma}_{JC}$  and  $\eta$  (effective plastic strain gradient) which is inversely proportional to the length of the primary

shear zone,  $L_p$ , representing the fundamental length scale governing the size effect when  $L_p$  reaches macro level  $\bar{\sigma} = \bar{\sigma}_{JC}$ . The constitutive material model for orthogonal machining is mainly based on the Taylor dislocation density model [25] which gives the shear flow  $\tau$  in terms of the total dislocation density  $\rho_T$  by Eq. (9).

$$\tau = \alpha G b \sqrt{\rho_T} \quad (9)$$

The total dislocation density  $\rho_T$  characterising the material hardening is the sum of two densities as flows:

$$\rho_T = \rho_s + \rho_g \quad (10)$$

where  $\rho_s$  characterises the Statistically Stored Dislocations (SSD), which is determined by the material test in the absence of strain gradient consideration according to the following equation

$$\rho_s = \left(\sigma_{ref} / M_t \alpha G b\right)^2 \quad (11)$$

The flow stress  $\sigma$  is related to the shear flow stress  $\tau$  by:  $\sigma = M_t \tau$ . Where  $M_t$  is the Taylor factor which acts as isotropic interpretation of the crystalline anisotropy at the continuum level. For FCC as well as for BCC metals that slip on {1 1 0} planes  $M_t$  is taken as 3.06 [26] and  $\sqrt{3}$  for an isotropic solid [27]. Whereas  $\rho_g$  concerns the Geometrically Necessary Dislocations (GND), which are required for compatible deformation of various parts of the nonuniformly deformed material. It is these GNDs and their effects on the flow stress that are considered in the present study. The flow stress  $\sigma$  in terms of dislocation densities can be expressed as:

$$\sigma = M_t \alpha G b \sqrt{\rho_s + \rho_g} \quad (12)$$

According to Ashby [28] the total density of dislocations  $\rho_T$ , which is given by the sum of statistically stored and geometrically necessary dislocations, is a special case of the following equation

$$\rho_T^\chi = \rho_s^\chi + \rho_g^\chi \text{ for } \chi = 1 \quad (13)$$

To properly estimate  $\rho_T$ , Ashby [28] has proposed that the exponent  $\chi$  (geometric factor defining the density of geometrically necessary dislocations (GNDs)) should be less than or equal to 1. Joshi and Melkote [4] believe that, due to large strain gradients commonly met in machining, a lower value of  $\chi$  is reasonable to introduce in Eq. (13). So, in the general case the material flow stress can be given by:

$$\sigma = M_t \alpha G b \sqrt{\rho_s^\chi + \rho_g^\chi} \quad (14)$$

Substituting Eq. (11) into Eq. (14), the flow stress can be written as (Eq. (15))

$$\sigma = \sigma_{ref} \sqrt{1 + (\rho_g / \rho_s)^2} \quad (15)$$

The density of geometrically necessary dislocations  $\rho_g$  is related to the gradient of plastic strain by

$$\rho_g = \bar{r} \frac{\eta}{b} \quad [28, 29].$$

Where  $\bar{r}$  is the Nye factor introduced

by Arsenlis and Parks [30] to reflect the effect of crystallography on the distribution of GNDs, and  $\bar{r}$  is around 1.90 for FCC polycrystals, 1.85 and 1.93 for bending and torsion, respectively [31]. Xinmin et al. [14] have considered its value as 2 for the case of machining. As discussed above that  $\sigma_{JC}$  is selected to be  $\sigma_{ref}$  the constitutive equation turns to be as follows

$$\sigma = \sigma_{JC} \sqrt{1 + (\bar{r} M_i^2 \alpha^2 G^2 b \eta / \sigma_{JC}^2)^2} \quad (16)$$

where  $\sigma_{JC}$  is the JC equivalent stress and  $\sigma_y$  is the yield stress.

From the works of Joshi and Melkote [4], the SG coefficient is obtained through the dislocation analysis of primary shear zone for micro scale machining, as follows

$$\eta = 1 / L_p \quad (17)$$

where  $L_p$  is the length of the primary shear zone which can be calculated by  $L_p = \frac{h(t)}{\sin \phi}$  with  $\phi$  is the primary shear angle (deg).

Finally, the constitutive equation can be expressed as:

$$\sigma = \sigma_{JC} \sqrt{1 + \left( \bar{r} M_i^2 \alpha^2 G^2 b / \sigma_{JC}^2 \left( \frac{h(t)}{\sin \phi} \right) \right)^2} \quad (18)$$

Since the strain gradient  $\eta$  is the inverse of  $L_p$ , it will decrease with the increase of  $h$ . This suggests that, when size variable  $L_p$  reaches to macro level, the flow stress calculated using Eq. (18) will be equal to that given by JC model (Eq. (2)).

In order to take into account the influence of SG-strengthening on the size effect phenomenon during down-cut peripheral milling simulations, the SG-based equivalent stress must be employed (Eq. (18)). Nevertheless, this theory is not available in the adopted FE analysis software. It is therefore necessary to implement the Eq. (18) with damage initiation (Eqs. (3) and (4)) and damage evolution models (Eqs. (5) - (7)) in the form of a user-defined stress update algorithm known as subroutine VUMAT formulated in ABAQUS®/EXPLICIT. After validating the pre-cited user routine, the constitutive equation including SG (Eq. (18)) was exploited.

### 3. Milling experiments

Down-cut peripheral milling experiments for a fixed  $f = 0.2$  mm/tooth and different  $V_C$ : 200, 400 and 600 m/min were performed on DMG, 3AXIS machining centre.

A Mitsubishi® milling tool ( $D_T = 22$  mm), refer-

enced 223WA20SA, with coated carbide insert referenced AOMT123608PEER-M was used. The geometry of the insert (Fig. 2, a) was measured by using an optical measuring device. This has helped to generate a 2D geometry of the insert (Fig. 2, b).

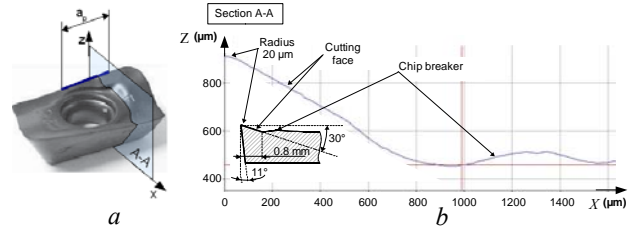


Fig. 2 Coated carbide insert used in experimentation a- 3D view b-Optical device generated 2D profile

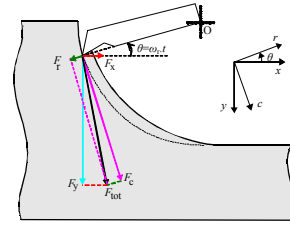


Fig. 3 Orthogonal down-cut milling force diagram

This insert profile was afterwards used in the FE model of milling (Fig. 1). While, workpiece is an aluminium alloy plate A2024-T351 with the thickness of 4 mm fixed on a standard dynamometer Kistler® 9257A. Fig. 5 shows the force diagram for orthogonal down-cut milling case. From the decomposition of forces, cutting force  $F_c$  acting tangentially to cutting speed  $V_C$  (m/min) can be calculated by Eq. (19).

$$\left. \begin{aligned} \vec{F}_{tot} &= F_x \vec{x} + F_y \vec{y} = F_c \vec{c} + F_r \vec{r} \\ \vec{F}_{tot} &= (F_x \sin \theta + F_y \cos \theta) \vec{c} + (F_x \cos \theta - F_y \sin \theta) \vec{r} \\ F_c &= F_x \sin \theta + F_y \cos \theta \end{aligned} \right\} \quad (19)$$

Eq. (20) was then used to calculate the SCE at various  $h$  values and cutting speeds. Afterwards these were compared with the corresponding numerical results.

$$SCE = F_c / h a_p \quad (20)$$

## 4. Results and analysis

This section discusses the contribution of various material strengthening factors in capturing size effect for orthogonal down-cut milling process. Numerical simulations at different cutting speeds and a fixed feed rate have been performed.

### 4.1. Temperature effect on material strengthening

To reveal the influence of temperature on the size effect, the evolution of the maximum secondary shear zone temperature calculated at various  $h$ , (without considering SG) for various cutting speeds has been presented in Fig. 4. It can be seen that, the lower the uncut chip thickness value, the lower the temperature of the secondary shear zone. However, for a given cutting speed; during the

decrease from macro to micro dimensions, the temperature decrease ( $\approx 30^\circ\text{C}$ ) is not significant enough to cause any considerable contribution in increasing material strengthening and influencing the size effect.

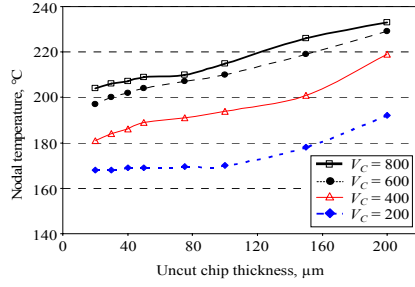


Fig. 4 Maximum secondary shear zone temperatures vs uncut chip thickness for various  $V_C$  (w/o SG)

#### 4.2. Strain rate hardening effect on material strengthening

Fig. 5 shows the plots of SCE for various  $h$  values at different  $V_C$  without considering SG. The partial capture of the size effect observed along the curves traced for all  $V_C$  is apparent. In addition, by increasing  $V_C$  up to 800 m/min a relatively higher capture of the size effect can be observed. This allows to further investigate the possible existence of a material strengthening mechanism other than SG-strengthening, tool edge radius effect (kept constant in this study) and temperature strengthening effects (not significant for the studied material as shown in subsection 4.1). Therefore, numerical results without considering SG concerning chip morphology were closely analysed at tool-chip interface for various  $h$  values. It can be seen from Fig. 6, which represents the simulated rake face-chip contact length  $L_C$  evolution at  $V_C = 200$  m/min.  $L_C$  initially decreases with a decrease in  $h$ . Afterwards,  $L_C$  starts to increase as  $h$  value further decreases toward micron level. A similar trend was observed when numerical simulations were performed for higher  $V_C$  (Fig. 7). In fact primary shear angle decreases as  $h$  decreases [32], further because of strain rate hardening, material strengthens. Under these conditions the chip has the tendency to straighten up rather than bend, so  $L_C$  increases. Nevertheless,  $L_C$  values were higher at analogous  $h$  values for higher  $V_C$ . This nonlinear increase in  $L_C$  at small  $h$  values implies that a higher energy is dissipated during frictional interaction at tool-workpiece interface, which yields to higher SCE. This provides an explanation for the partial capture of the size effect even without SG-strengthening as it was demonstrated in Fig. 5. This trend of increase in  $L_C$  is consistent with the results of Liu and Melkote [7], when a sharp tool is replaced by an edged radius tool.

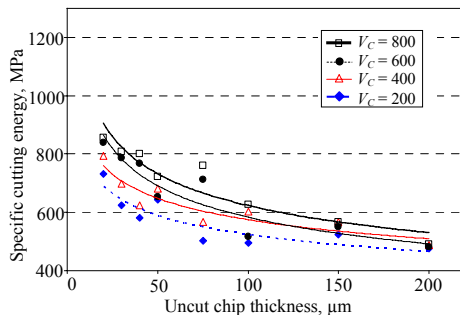


Fig. 5 Specific cutting energy evolution at various uncut chip thickness values (w/o SG)

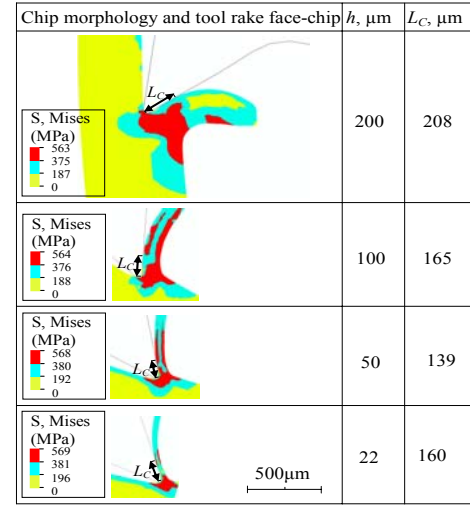


Fig. 6 Simulated tool rake face-chip contact length ( $\mu\text{m}$ ) for  $V_C = 200$  m/min (w/o SG)

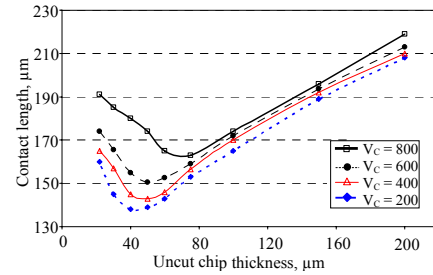


Fig. 7 Simulated tool rake face-chip contact lengths (w/o SG) at various uncut chip thickness for various  $V_C$

It can be seen in Fig. 7 that for all cutting speeds rake face-chip contact lengths initially decrease with the decrease in  $h$  value. Afterwards,  $L_C$  starts to increase as  $h$  value further decreases to micro level. As, tool edge radius was unchanged for all cutting simulations, therefore this increase in tool-chip contact lengths at smaller  $h$  values, resulting in higher SCE can be attributed to highly strain rate dependent properties of the studied material. Simultaneously, it is noticeable that length scale (in term of uncut chip thickness) at which  $L_C$  starts to increase; for lower  $h$  values, varies with cutting speeds. Indeed, when  $V_C$  evolves from 200 to 400, 600 and 800 m/min, length scale increases from 44 to 46  $\mu\text{m}$ , 48 and 60  $\mu\text{m}$ , respectively. Kountanya [32] has noted this length scale value as 42.1  $\mu\text{m}$  for  $V_C = 56.4$  m/min in his research work on the same material studied in the present paper.

Insight analysis of both Fig. 7 and the result of Kountanya [32] show that the length scale increases with the increase in cutting speed, however this increase is remarkable for higher cutting speeds ( $\geq 800$  m/min). This is consistent with the findings of Liu and Melkote [7], though they have attributed this increase in the length scale to the temperature drop in secondary shear zone for a strain rate insensitive aluminium alloy Al5083-H116. It can be deduced from above discussion that, independent of material properties the higher the cutting speed, the higher the nonlinear length scale (in term of uncut chip thickness). Though the reasons of this increase could be different; either temperature drop in secondary shear zone for a strain rate insensitive material [7] or strain hardening properties of a strain rate sensitive material.

### 4.3. Strain gradient effect on material strengthening

Further, to study the contribution of SG-strengthening on the size effect for strain rate sensitive material, cutting simulations considering SG-model (Eq. (18)) were performed for various  $V_C$ . Fig. 8 presents the SCE plots with and without considering SG-effects for various  $h$  values at different cutting speeds. It can be noted that the SCE values computed in the case of a simulation considering SG are closer to experimental ones than that calculated without considering SG. This proves that the modified JC law (Eq. (18)) allows a good estimation of the cutting force during the variation of the  $h$  from macro to micro level. Moreover, for lower  $h$ , the latter law permits to capture the nonlinear increase in SCE whose evolution is more pronounced than that calculated without considering SG.

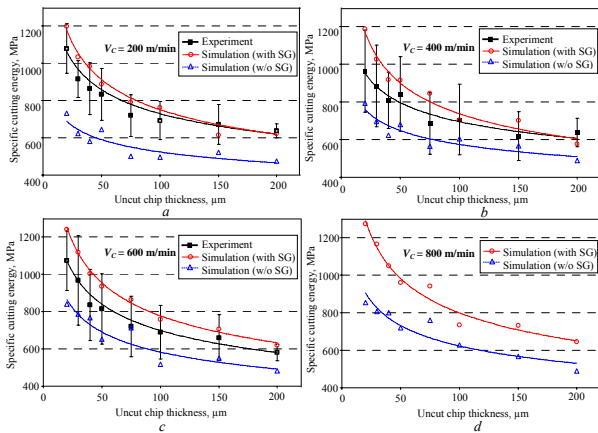


Fig. 8 SCE evolution vs  $h$  values at different  $V_C$ : a -  $V_C = 200$  m/min, b -  $V_C = 400$  m/min, c -  $V_C = 600$  m/min, d -  $V_C = 800$  m/min (here experimental force were not registered)

However, it is interesting to underline that, the results shown in Fig. 8 depict that even at large  $h$  (e.g.  $h = 200 \mu\text{m}$ ), the difference between the models (with and without considering SG) is still very large, which seems not to be easily explained by microstructural effects. By plugging in numbers into Eq. (18), one finds that the effect of the SG vanishes at unphysically large values of  $L_P$  (roughly 1 m). Nevertheless, this difference (at  $h = 200 \mu\text{m}$ ) becomes negligible if compared with the one obtained at very small values of  $h$  (where specific cutting energy increases exponentially [10, 15]) around  $0.25R_n = 5 \mu\text{m}$  or even lesser, while in present study the simulation have been run up to  $22 \mu\text{m}$  ( $\approx R_n$ ). This helps to infer that physical significance of this model (Eq. (18)) prevails mainly at  $h$  values of the order of  $R_n$  and below.

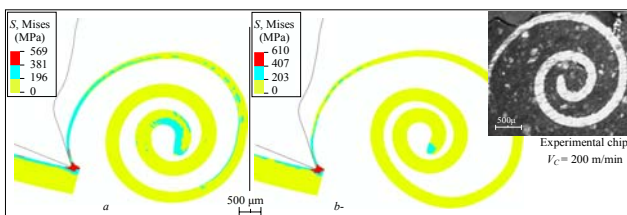


Fig. 9 Von Mises stress plots at  $h = 22 \mu\text{m}$  and  $V_C = 200$  m/min a) w/o SG b) with SG

Fig. 9 shows the von Mises stress plot for cutting speeds of 200 m/min. The chip morphologies with and without considering SG-strengthening effects present globally, a certain similarity and are comparable with the experimental one.

From stress point of view, it can be observed that by introducing SG-effects in the material model, and when  $V_C$  is equal to 200 m/min, the maximum von Mises stresses have been increased from 569 to 610 MPa. Whereas, for a higher  $V_C$  of 800 m/min, maximum stresses were increased from 586 to 653 MPa. The increments in stress magnitude for both cutting speeds are comparable, approximately. This suggests that SG-hardening is the dominant phenomenon for material strengthening at high  $V_C$  and lower  $h$  values for a strain rate dependant material. To fully capture the size effect for micro cutting operations, SG-based strengthening mechanism is inevitable.

## 5. Conclusions

The present study proposes a physical comprehension of material strengthening factors that contribute to the size effect in micro-cutting operations. Orthogonal down-cut milling case for a strain rate sensitive aluminium alloy material A2024-T351 has been investigated. The important conclusions of this study could be underlined as:

1. During down-cut milling, tool-chip contact length  $L_C$  decreases with the reduction of uncut chip thickness  $h$  until it reaches a certain value. After that, this contact length increases as  $h$  decreases to micro dimensions. This increase, in  $L_C$ , implies that the well-known minimum cutting chip thickness is reached and a higher energy is dissipated during frictional interaction at tool-chip interface, resulting in higher specific cutting energy.

2. Similar trend concerning tool-chip contact length variation regarding uncut chip thickness was observed for all studied cutting speeds ( $V_C$ ). Nevertheless, in the micro-level the length scale at which the lengths of rake face-chip contact start to increase proportionally to  $V_C$ . The higher the  $V_C$ , the higher the length scales.

3. The implementation of a modified Johnson-cook material model via a user subroutine VUMAT in the commercial software ABAQUS®/EXPLICIT has allowed to analyze accurately the contribution of the strain gradient-based hardening on the size effect phenomenon at micro cutting level.

4. The increments in the maximum von Mises stress magnitudes using strain gradient-based plasticity model, for various  $V_C$ , are more or less the same. This suggests that strain gradient hardening is the dominant phenomenon for material strengthening at high  $V_C$  and lower uncut chip thickness for the studied material.

5. Specific cutting energy values obtained by numerical simulations, using strain gradient-based plasticity model, were quite close to the experimental ones. This shows that, to fully capture the size effect during micro cutting operations, strain gradient-strengthening mechanism can not be ignored; even at high cutting speeds and for strain rate dependent materials.

Finally, this contribution permits to a close multi-scale physical understanding of the role of various strengthening factors contributing to the size effect. Potentially, this will allow improving the existing cutting models and help to capture events happening at micro-levels.

## References

1. **Backer, W.R.; Marshall, E.R.; Shaw, M.C.** 1952. The size effect in metal cutting, *Transaction of ASME* 74: 61-72.
2. **Larsen-Basse, J.; Oxley, P.L.B.** 1973. Effect of strain rate sensitivity on scale phenomena in chip formation. In *Proceedings of 13<sup>th</sup> International Machine Tool Design and Research Conference*: 209-216.
3. **Dinesh, D.; Swaminathan, S.; Chandrasekar, S.; Farris, T.N.** 2001. An intrinsic size effect in machining due to the strain gradient. In *Proceedings of ASME IMECE*: 197-204.
4. **Joshi, S.S.; Melkote, S.N.** 2004. An explanation for the size-effect in machining based on strain gradient plasticity, *Journal of Manufacturing Science and Engineering* 126(4): 679-684.
5. **Armarego, E.J.A.; Brown, R.H.** 1962. On the size effect in metal cutting, *International Journal for Production Research* 1(3): 75-99.
6. **Nakayama, K.; Tamura, K.** 1968. Size effect in metal cutting force, *Journal of Engineering for Industry* 90(1): 119-126.
7. **Liu, K.; Melkote, S.N.** 2007. Finite element analysis of the influence of tool edge radius on size effect in orthogonal micro-cutting process, *International Journal of Mechanical Science* 49(5): 650-660.
8. **Thomsen, E.G.; Lapsley, J.T.; Grassi, R.C.** 1953. Deformation work absorbed by the workpiece during metal cutting, *Transactions of ASME* 75: 591-603.
9. **Albrecht, P.** 1960. New developments in the theory of metal cutting process: Part-I the ploughing process in metal cutting, *Journal of Engineering for Industry* 82: 348-357.
10. **Liu, K.; Melkote, S.N.** Material strengthening mechanisms and their contribution to size effect in micro-cutting. -*Journal of Manufacturing Science and Engineering*, 2006, 128(3), p.730-738.
11. **Kim, K.W.; Lee, W.Y.; Sin, H.C.** 1999. A finite element analysis of machining with the tool edge considered, *Journal of Material Processing Technology* 86(1-3): 45-55.
12. **Fnides, B.; Yallese, M.A.; Mabrouki, T.; Rigal, J.F.** 2009. Surface roughness model in turning hardened hot work steel using mixed ceramic tool, *Mechanika* 3(77): 68-73.
13. **Ryynänen, V.; Ratava, J.; Lindh, T.; Rikkonen, M.; Sihvo, I.; Leppänen, J.; Varis, J.** 2009. Chip control system for monitoring the breaking of chips and elimination of continuous chips in rough turning, *Mechanika* 4(78): 57-62.
14. **Xinmin, L.; Hongtao, L.; Chengfeng, L.; Zhongqin, L.; Jun, N.** 2008. Modelling and analysis of micro scale milling considering size effect, micro cutter edge radius and minimum chip thickness, *International Journal of Machine Tools and Manufacture* 48(1): 1-14.
15. **Mabrouki, T.; Rigal, J.-F.** 2006. A contribution to a qualitative understanding of thermo-mechanical effects during chip formation in hard turning, *Journal of Material Processing Technology* 176(1-3): 214-221.
16. **Subbiah, S.; Melkote, S.N.** 2008. Effect of finite edge radius on ductile fracture ahead of the cutting tool edge in micro-cutting of Al2024-T3, *Material Science and Engineering A* 474(1-2): 283-300.
17. **Zorev, N.N.** 1963. Interrelationship between shear processes occurring along tool face and on shear plane in metal cutting, *International Research in Production Engineering*: 42-49.
18. **Ni, W.; Cheng, Y.T.; Weiner, A.M.; Perry, T.A.** 2006. Tribological behaviour of diamond-like-carbon (DLC) coatings against aluminium alloys at elevated temperatures, *Surface and Coatings Technology* 201(6): 3229-3234.
19. **Asad, M.; Mabrouki, T.; Rigal, J.-F.** 2010. Finite-element-based hybrid dynamic cutting model for aluminium alloy milling. *Proceedings of IMechE Part b: Journal of Engineering Manufacture* 224(1): 1-13.
20. **Johnson, G.R.; Cook, W.H.** 1985. Fracture characteristics of three metals subjected to various strains, strain rates, temperatures and pressures, *Engineering Fracture Mechanics* 21(1): 31-48.
21. **Hillerborg, A.; Modeer, M.; Petersson, P.E.** 1976. Analysis of crack formation and crack growth in concrete by means of fracture mechanics and finite elements, *Cement Concrete Research* 6: 773-782.
22. **Teng, X.; Wierzbicki, T.** 2006. Evaluation of six fracture models in high velocity perforation, *Engineering Fracture Mechanics* 73: 1653-1678.
23. <http://www.knovel.com> (date access 05-06-2008).
24. **Xue, Z.; Huang, Y.; Li, M.** 2002. Particle size effect in metallic materials: a study by the theory of mechanism-based strain gradient plasticity, *Acta Materialia* 50(1): 149-160.
25. **Taylor, G.I.** 1934. The mechanism of plastic deformation of crystals, Part I.—Theoretical. *Proceedings of Royal Society* 145: 362-387.
26. **Kocks, U.F.** 1970. The relation between polycrystal deformation and single crystal deformation, *Metallurgical and Material Transactions* 1: 1121-1144.
27. **Liu, B.; Huang, Y.; Li, M.; Hwang, K.C.; Liu, C.** 2005. A study of the void size effect based on the Taylor dislocation model, *International Journal of Plasticity* 21(11): 2107-2122.
28. **Ashby, M.F.** 1970. The deformation of plastically non-homogeneous alloys, *Philosophy Magazine*, 21: 399-424.
29. **Huang, Y.; Xue, Z.; Gao, H.; Nix, W.D.; Xia, Z.C.** 2000. A study of micro-indentation hardness tests by mechanism-based strain gradient plasticity, *Journal of Material Research* 15: 1786-1796.
30. **Arsenlis, A.; Parks, D.M.** 1999. Crystallographic aspects of geometrically-necessary and statistically-stored dislocation density, *Acta Materialia* 47: 1597-1611.
31. **Shi, G.; Deng, X.; Shet, C.** 2004. The *J*-integral and geometrically necessary dislocations in non uniform plastic deformation, *International Journal of Plasticity* 20(8): 1739-1762.
32. **Atkins, A.G.** 2003. Modeling metal cutting using modern ductile fracture mechanics: quantitative explanations for some longstanding problems, *International Journal of Mechanical Science* 45(2): 373-396.

M. Asad, T. Mabrouki, F. Girardin, Y. Zhang, J.-F. Rigal

FIZIKINIO MEDŽIAGOS SUSTIPRĖJIMO  
FAKTORIAUS MAKRO IR MIKRO FREZAVIMO  
METU PAGRINDIMAS

Re z i u m ė

Šiame straipsnyje apibūdinamos medžiagos deformacinio sustiprėjimo charakteristikos, kaip reikšmingas faktorius didinant medžiagos stiprumą, kai frezavimo metu nupjautos drožlės storis mažėja nuo makro iki mikro dydžio. Tai buvo nustatyta apdirbant deformacijos greičiui jautrią medžiagą (A2024-T351), kai danties priekinio paviršiaus ir drožlės kontakto ilgis netiesiškai didėja, įrankio nupjaunamos drožlės storiui artėjant prie mikro dydžio. Dėl trinties tarp danties ir drožlės sunaudojama daug energijos, padidėja specifinė pjovimo energija. Be to, tyrimas rodo, kad padidėjus pjovimo greičiui padidėja danties priekinės plokštumos ir drožlės kontakto ilgis. Analizuojant deformacinio stiprėjimo gradiento įtaką efekto dydžiui, atliekant mikropjovimo operacijas modifikuotas Johnsono ir Cook medžiagos (deformacijos gradientu paremta prielaida) ekvivalentinių įtempių modelis buvo pasiūlytas naudoti ABAQUS®/EXPLICIT taikant įdiegtą programą VUMAT. Rezultatai atskleidė deformacinio stiprėjimo gradiento reikšmę visam mikropjovimo operacijos dydžio efekto fenomenui, esant deformacijos greičiui jautriai medžiagai ir dideliame pjovimo greičiui. Galutiniais frezavimo eksperimentais siekta skaitiniu būdu patvirtinti, specifinės pjovimo energijos ir drožlės morfologijos modelį.

M. Asad, T. Mabrouki, F. Girardin, Y. Zhang, J.-F. Rigal

TOWARDS A PHYSICAL COMPREHENSION OF  
MATERIAL STRENGTHENING FACTORS DURING  
MACRO TO MICRO-SCALE MILLING

S u m m a r y

Present work highlights the importance of material strain rate hardening characteristics as an influential factor in increasing material strength, as uncut chip thickness decreases from macro to micro-level dimensions during down-cut milling process. It has been found for a strain rate dependent material (A2024-T351) that rake face-chip contact length increases nonlinearly when tool approaches to micro-level of uncut chip thickness. This suggests higher energy consumption due to frictional interaction at tool-chip interface, resulting in higher specific cutting energy. In addition, results depict that increase in cutting speeds are attributed to increased rake face-chip contact lengths. Furthermore, to analyze the contribution of

the strain gradient hardening on size effect phenomenon during micro cutting operations, modified Johnson-Cook material model (strain gradient-based approach) of the equivalent stress has been formulated in ABAQUS®/EXPLICIT via its user subroutine VUMAT. The results put forward the significance of strain gradient hardening to fully capture the size effect phenomenon during micro cutting operations, at high cutting speeds for a strain rate dependent material. Finally, milling experiments have been performed to validate the numerical model in terms of specific cutting energy and chip morphology.

М. Асад, Т. Маброуки, Ф. Гирардин, И. Зханг,  
Ю.-Ф. Ригал

О ФИЗИЧЕСКОМ ОБЪЯСНЕНИИ ФАКТОРА  
УПРОЧНЕНИЯ МАТЕРИАЛА ПРИ МАКРО- И  
МИКРОФРЕЗЕРОВАНИИ

Р е з ю м е

Статья объясняет характеристики деформационного упрочнения материала, как особый фактор увеличения прочности материала, когда толщина удаляемой стружки уменьшается от макро- до микро величины во время обработки фрезерованием. Это определено для материала, чувствительного к скорости деформации (A2024-T351), когда длина контакта передней поверхности зуба и стружки возрастает нелинейно при приближении инструмента к микро толщине снимаемой стружки. Это требует значительной энергии из-за трения в контакте инструмента и стружки и повышает специфическую энергию резания. Кроме того, исследования показывают, что повышенная скорость резания увеличивает длину контакта передней поверхности со стружкой. При анализе вклада градиента деформационного упрочнения на величину эффекта при микро резании модифицированный метод эквивалентных напряжений материала (предпосылка обоснована градиентом деформации) был предложен используя ABAQUS®/EXPLICIT с помощью подпрограммы VUMAT. Результаты выделили значение градиента деформационного упрочнения для полного феномена величины эффекта операции микро резания при высокой скорости резания для материала, чувствительного к скорости деформации. Конечные результаты экспериментов фрезерования были проведены для утверждения численной модели специфической энергии резания и морфологии стружки модели.

Received September 08, 2010

Accepted February 07, 2011